Appl. Math. Mech. -Engl. Ed., **42**(6), 871–884 (2021)

APPLIED MATHEMATICS AND MECHANICS (ENGLISH EDITION)

https://doi.org/10.1007/s10483-021-2734-6

Numerical method for simulating rarefaction shocks in the approximation of phase-flip hydrodynamics*

M. M. BASKO†

Keldysh Institute of Applied Mathematics, Russian Academy of Sciences,
Miusskaya Square 4, Moscow 125047, Russia

(Received Jul. 23, 2020 / Revised Jan. 31, 2021)

Abstract A finite-difference algorithm is proposed for numerical modeling of hydrodynamic flows with rarefaction shocks, in which the fluid undergoes a jump-like liquid-gas phase transition. This new type of flow discontinuity, unexplored so far in computational fluid dynamics, arises in the approximation of phase-flip (PF) hydrodynamics, where a highly dynamic fluid is allowed to reach the innermost limit of metastability at the spinodal, upon which an instantaneous relaxation to the full phase equilibrium (EQ) is assumed. A new element in the proposed method is artificial kinetics of the phase transition, represented by an artificial relaxation term in the energy equation for a "hidden" component of the internal energy, temporarily withdrawn from the fluid at the moment of the PF transition. When combined with an appropriate variant of artificial viscosity in the Lagrangian framework, the latter ensures convergence to exact discontinuous solutions, which is demonstrated with several test cases.

Key words fluid dynamics with phase transitions, two-phase flow, rarefaction shock, Lagrangian scheme, artificial viscosity, artificial kinetics

Chinese Library Classification O362
2010 Mathematics Subject Classification 76T10, 76L05, 76M20, 35L67

1 Introduction

In many cases where the equations of hydrodynamics are used to model experiments, the thermodynamic trajectories of at least some fluid elements pass through the liquid-gas phase coexistence region. Numerous examples can be found in analyses of laser-irradiated targets[1–4] and studies on cavitation and spallation in fluids[5–8]. A simple and universal approach, often adopted in such situations[2,4,9–10], is to stay within the framework of one-fluid hydrodynamics and use the fully equilibrium equation of state (EQ EOS) obtained by applying the Maxwell rule to the "parental" equation of state (EOS) of the van der Waals type, which has a region of absolute thermodynamic instability below the spinodal curve. However, because the EQ EOS is based on the assumption of instantaneous gas-liquid equilibration in the phase coexistence region, i.e., everywhere below the binodal curve, and allows no negative pressure, it becomes

* Citation: BASKO, M. M. Numerical method for simulating rarefaction shocks in the approximation of phase-flip hydrodynamics. *Applied Mathematics and Mechanics* (*English Edition*), **42**(6), 871–884 (2021) https://doi.org/10.1007/s10483-021-2734-6

† Corresponding author, E-mail: mmbasko@gmail.com

a poor approximation for very fast processes such as target responses to sub-nanosecond laser pulses and is fully unsuitable for modeling spallation and cavitation.

As an opposite alternative, aimed specifically at modeling fast hydrodynamic processes where the thermodynamic trajectories penetrate deeply into the region of metastable (MS) states and negative pressures, the approximation of phase-flip (PF) hydrodynamics can be used[11]. This approximation is based on the assumption that, having entered the phase coexistence region, each fluid element continues to obey the parental MS EOS all the way down to the spinodal, where an instantaneous and irreversible transition to the EQ EOS takes place. Such an assumption is justified by a very rapid, explosion-like increase in the rate of homogeneous nucleation in the immediate vicinity of the spinodal[12–15]. A similar idea was put forward by Grady[16] for modeling spall fractures in liquids. However, unfortunately, it has not been pursued any further. In comparison with other methods for modeling MS fluids, the PF hydrodynamics has the advantages of being much simpler than, for example, the multi-phase hydro-kinetic models (see Refs. [17] and [18] and the references therein) and having much less computational demand than the molecular dynamics (MD) simulation[19–20]. In addition, it admits exact solutions[11], which is valuable for gaining insight into the dynamics of MS fluids as well as for calibrating numerical methods.

For practical applications, one certainly needs a discretized version of the PF hydrodynamics. However, a non-trivial obstacle to constructing a finite-difference approximation arises due to a new type of flow discontinuity introduced by the assumed instantaneous decay of MS states. On the one hand, any such PF discontinuity represents a material interface in the sense that it separates two different thermodynamic phases, whose properties are calculated from two different EOS branches. On the other hand, its propagation in space is not directly coupled to the fluid motion: in some cases (like the one treated in this paper) it may coincide with a shock front, while in others (like in spall fragmentation fronts) it may propagate much faster than any Hugoniot shock. Hence, many modern algorithms developed recently for multi-phase flows (see, for example, Refs. [21]–[23] and the references therein) become of little help in our case, for which even the pertaining two-phase Riemann problem has not been addressed.

As a first attempt to produce a workable numerical algorithm, we explore one of the simplest approaches based on the ideas similar to those put forward about 60 years ago for modeling strong shocks. The proposed method is based on a combination of a specially adjusted variant of artificial viscosity with a relaxation term for a "hidden" internal energy, artificially withdrawn from the fluid at the moment of the PF transition. In other words, the key new ingredient in our scheme is a kind of artificial kinetics of phase transition which, by analogies with the artificial viscosity smearing shock fronts in space, smears the instantaneous phase transition in time. We restrict our treatment to the Lagrangian framework, where no need for either interface tracking or phase mixing arises, while the implementation of the phase transition criterion is pretty straightforward. The method is tested against the exact solution from Ref. [11] in the parameter range where the decaying MS states on the spinodal have positive pressures and, as a consequence, the expanding fluid passes through a rarefaction shock front. The applications to cavitation and spallation initiated by negative spinodal pressures will be discussed elsewhere.

All the illustrative examples and test cases below are calculated by using a generalized van der Waals equation of state (GWEOS)[24–26] of the form

$$p(v,\theta) = \frac{(\kappa-\kappa^{-1})\theta}{v-\kappa^{-1}} - \frac{\kappa}{v^n}, \tag{1}$$

$$e(v,\theta) = c_V(\kappa-\kappa^{-1})\theta - \frac{1}{2}\kappa(\kappa-1)v^{1-n}, \tag{2}$$

where $\kappa = (n+1)/(n-1)$, while the exponent n (>1) and heat capacity c_V (>0) are two independent free parameters of the GWEOS. Everywhere throughout this paper, the values

$n = c_V = 1.5$ are used. The EOS (1), (2) is given in its reduced form, where the pressure p, the specific volume $v \equiv \rho^{-1}$, and the temperature θ are measured in units of the corresponding critical values $P_{\rm cr}$, $V_{\rm cr} = \rho_{\rm cr}^{-1}$, and $T_{\rm cr}$. The mass-specific internal energy e is in units of $P_{\rm cr}V_{\rm cr}$. The dimensional quantities $P_{\rm cr}$, $V_{\rm cr}$, and $T_{\rm cr}$ are three additional free parameters of the GWEOS. For more details, one may see Refs. [11] and [26].

The rest of this paper is organized as follows. In Section 2, our principal reference case of a rarefaction shock inside a plane-parallel release wave is briefly described, and the results of the numerical tests for the classical von Neumann-Richtmyer artificial viscosity are discussed. Subsection 3.1 introduces the proposed method of artificial smearing in time of the MS→EQ phase jump by an artificial energy relaxation term, and Subsection 3.2 presents the results of the numerical tests of the advocated algorithm against the exact solution from Ref. [11]. Finally, the main conclusions are summed up in Section 4.

2 Artificial viscosity for rarefaction shocks in the PF hydrodyanmics

2.1 General considerations

Consider a fluid flow where some fluid elements pass through the liquid-gas phase coexistence region. If the initial state O lies outside the two-phase region, a typical thermodynamic trajectory of such a fluid element may look like the OBD curve on the (v, p) plane of Fig. 1: Start from point O, then enter the two-phase region upon crossing the binodal at point B, and finally reaches the spinodal at point D. Note that the intersection points B and D can both lie either on the liquid branches of the binodal and spinodal or on their vapor branches. If the considered flow is simulated with a Lagrangian hydrodynamics code, the trajectory OBD may represent the evolution of the thermodynamic state in any fixed mesh cell.

The key assumption in the PF approximation is that the fluid motion is described by the usual system of single-phase hydrodynamics equations (for example, Eqs. (A2)–(A5) in the case of one-dimensional (1D) planar flows), and only the algorithm for applying the EOS is modified.

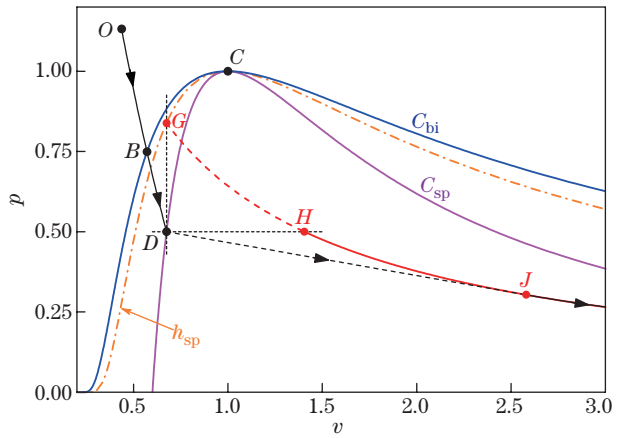

Fig. 1 Thermodynamic (v, p) plane of a fluid with a liquid-gas phase transition, where $C_{\rm bi}$ and $C_{\rm sp}$ denote the binodal and the spinodal curves, respectively, and C denotes the critical point. The trajectory of the fluid elements in a self-similar flow by expansion into a vacuum is shown schematically as a thin black curve $OBDJ$ with arrows. The thick red curve GHJ is the PF Hugoniot constructed for the initial state D. In the rarefaction shock, the fluid state jumps from D to J. The GH segment of the PF Hugoniot between the isochoric and isobaric PFs is unphysical. The dash-dotted curve $h_{\rm sp}$ (orange) is the locus of the isochoric post-flip states G as the initial state D slides along $C_{\rm sp}$ (color online)

More specifically, it is assumed that the fluid obeys the parental MS EOS (1), (2) everywhere above the binodal curve and over the entire metastability region, i.e., all the way down to point D, where there is an instantaneous irreversible transition (PF), to the EQ EOS branch; the EQ EOS in the form of $p_{\mathrm{EQ}}(v,\theta)$ and $E_{\mathrm{EQ}}(v,\theta)$ is obtained from Eqs. (1) and (2) by applying the Maxwell rule to every isotherm with a given θ[26]. In this approach, there is no need to introduce extra differential equations to describe the phase separation in a moving fluid: in Lagrangian variables, it is readily achieved with an easily traceable binary marker, indicating which EOS branch (MS or EQ) is used in a given fluid element at a given time.

Without any a priori knowledge about the global properties of the flow, one has to assume that the PF transition in a given Lagrangian element (cell) occurs at fixed values of the specific volume v and the specific internal energy e. This condition determines uniquely the post-flip state G for any given pre-flip state D on the spinodal. The locus of all possible isochoric post-flip states is given by the curve h_{sp} in Fig. 1. Thus, the formulated rule appears to provide a clear recipe for implementation of the PF into a Lagrangian code: one tracks the evolution of the thermodynamic state in each mesh cell, and performs an isochoric MS→EQ PF in that cell at any time the spinodal is being crossed from its MS side.

The problem with such a "single-leap" approach is a significant pressure jump (of the order of P_{cr}), caused by an isochoric PF in an individual cell. When separated in time, such pressure jumps in different cells tend to generate violent spurious oscillations in a simulated flow. This behavior closely resembles what happens when one tries to simulate compression shocks without artificial viscosity[27]. The analogy becomes even more conspicuous when one considers the exact PF solution for a release wave by expansion into a vacuum[11], which we adopt as our principal reference case and where the PF occurs inside a rarefaction shock front.

As an initially uniform half-space $x < 0$ of a fluid at a positive pressure is released into a vacuum, the resulting flow is described by a self-similar centered rarefaction wave (CRW) for any EOS[28–29]. In this solution, the dependent variables for the density, pressure, and velocity are functions of a single self-similar variable $\xi = x/t$. Hence, all the elements of the expanding fluid follow one and the same thermodynamic trajectory, whose initial segment OBD above the spinodal is an MS isentrope. If the initial entropy is high enough to ensure a positive pressure $p_D > 0$ on the spinodal, the zero pressure at the outer boundary causes the fluid state to jump from D to the Chapman-Jouguet point J, lying on the expansion branch GHJ (see Fig. 1) of the PF Hugoniot[11]. In the coordinate space (see Figs. 2–7), the state D is represented by the finite segment D_+D_- of a constant flow, i.e., the spinodal shelf. A distinctive feature of the PF Hugoniot is that all the post-jump states are calculated by using a different (EQ) EOS branch as compared with the pre-jump state D. The post-jump state J has a lower (but always positive) pressure $0 < p_J < p_D$, a larger specific volume $v_J > v_D$, and a higher specific entropy $s_J > s_D$. Passing through such a rarefaction front, the fluid experiences a jump-like acceleration towards the vacuum. Behind the front, the flow evolves along the EQ isentrope starting at J.

The history of successful application of the method of artificial viscosity to modeling the compression shocks[27,30] suggests that it could be tried for the PF rarefaction shocks as well. One might expect that any pressure jump, accompanying an isochoric PF (the $D \to G$ jump in Fig. 1), would be quickly dissipated by the artificial viscosity, with the flow eventually settling down to the correct profile below the Chapman-Jouguet point J.

In this work, we investigate the classical combination of the linear and quadratic terms[30–31]

$$q = -\mu_1 \rho c_{\mathrm{s}} \Delta x \frac{\partial u}{\partial x} - \mu_2 \rho (\Delta x)^2 \left|\frac{\partial u}{\partial x}\right| \frac{\partial u}{\partial x} \tag{3}$$

in the viscous contribution q to the pressure p, where u is the flow velocity, c_{s} is the adiabatic speed of sound, Δx is the width of the grid cell where q is calculated, and μ_1 and μ_2 are two non-negative dimensionless coefficients of the order of unity. Equation (3) is written for the

1D planar flows, to which all our test cases belong. The specific numerical scheme, used in the simulations, is described in Appendix A.

2.2 Numerical tests for artificial viscosity

Test simulations have been performed for a planar fluid layer, initially occupying the interval $0 < x < 1$ in a uniform thermodynamic state (v_0, θ_0), with $p_0 = p(v_0, \theta_0)$ and $e_0 = e(v_0, \theta_0)$ given by Eqs. (1) and (2). The boundary conditions were the rigid reflecting wall at $x = 0$ and the zero pressure at the right expanding boundary with vacuum at $x \geqslant 1$. Each simulation had been stopped before the rarefaction wave arrived at $x = 0$, so that the left boundary had no effect on the analyzed flow pattern.

To mitigate the finite-difference perturbation, introduced by the initial discontinuity at $x = 1$, we use a Lagrangian grid that is refined towards the vacuum boundary. The grid is set by an initial partition $\{x_j\}$ of the $0 < x < 1$ interval such that the cell width $\Delta x_{j+1/2} \equiv x_{j+1} - x_j$ remains constant $\Delta x_{j+1/2} = h_0$ for $0 < x < 0.5$ and monotonically decreases in geometric progression from h_0 to $h_1 \approx 0.02 h_0$ as x increases from 0.5 to 1. The simulation results are discussed for two cases: (i) a coarse grid with $h_0 = 0.01$ and a total of $N = 250$ cells over the combined interval $x \in [0, 1]$ and (ii) a fine grid with $h_0 = 0.002\,5$ and a total of $N = 1\,000$ cells over the combined interval $x \in [0, 1]$.

Figure 2 compares the density and pressure profiles, calculated for different combinations of the viscosity parameters in Eq. (3), with the exact solution from Ref. [11]. The pre-flip isentrope OD_+ is specified by fixing the initial density at $\rho_0 = 1.75$ and the spinodal pressure at $p_D = 0.5$. The profiles are shown for the moment $t = 0.25$ when the head of the CRW wave (point O in Fig. 2) arrives at $x = 0.168$.

Firstly, we examine two different variants of the pure quadratic viscosity with $\mu_1 = 0$ and $\mu_2 = 2$, i.e., the commonly used von Neumann-Richtmyer-Rosenbluth (NRR) viscosity[27], which acts by compression only and is set to be equal to zero in the expanding cells with $\Delta u_{j+1/2} \equiv u_{j+1} - u_j \geqslant 0$, and the von Neumann-Richtmyer (NR) viscosity (originally proposed in Ref. [32]), which remains non-zero for any non-zero values of $\Delta u_{j+1/2}$. Figure 2 demonstrates that both these variants perform rather poorly, with the entire flow section below point D_+ being afflicted by strong cell-to-cell fluctuations. Here, the perturbations, generated by the pressure jumps near the shock front D_-J, propagate freely upstream across the entire region of the constant flow on the spinodal shelf D_+D_- because the fluid enters the shock front at D_- with a subsonic velocity $u_D - \xi_{D_-} = c_{sJ}(v_D/v_J) < c_{sD}$, where c_{sD} and c_{sJ} are, respectively,

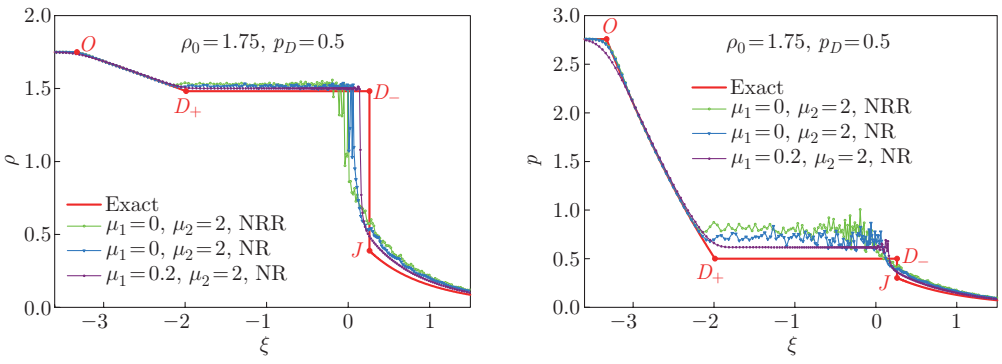

(a) Density (b) Pressure

Fig. 2 Density and pressure profiles in the CRW solution along the self-similar coordinate $\xi = (x - 1)/t$, calculated with different options of the artificial viscosity (3). The expansion isentrope starts at the initial density $\rho_0 = 1.75$, and reaches the liquid spinodal branch at pressure $p_D = 0.5$. In the exact solution (red), the single point D of Fig. 1 is represented by the constant-flow segment D_+D_- (color online)

the MS and EQ sound speeds at points D and J. When the NRR and NR viscosity options are compared between themselves, the NR version with a non-zero dissipation under both compression and expansion is a clear winner, which is not a surprise as we are dealing with a rarefaction shock.

Secondly, we note that the small-amplitude fluctuations, surviving the quadratic viscosity, can be further suppressed by adding a non-zero linear viscosity component. A series of tests have confirmed that the NR compression-expansion viscosity (3) with μ_1, which is approximately larger than 0.1, is sufficient for ensuring smooth and stable flow profiles, except for a narrow region upstream from the shock front, where several prominent oscillations with a period of 5–7 mesh cells are always observed (see Figs. 2 and 3). As these oscillations propagate upstream, they are rapidly damped by the linear viscosity. As a robust compromise, the coefficients in Eq. (3) were fixed at $\mu_1 = 0.2$ and $\mu_2 = 2$ for all subsequent simulations. Beside the artificial viscosity, the smoothness of the numerical profiles is slightly affected by the value of the CFL number L (see Eq. (A12)), especially as the latter approaches the stability limit. All the results of this work were simulated with a safe margin of $L = 0.1$.

Though fairly effective in suppressing spurious fluctuations, the artificial viscosity does not, unfortunately, ensure convergence to the exact solution. Figure 3 clearly demonstrates that, as the grid resolution is increased, our numerical solution approaches a flow profile which deviates significantly from the exact solution all along the spinodal shelf and behind the shock front. The absence of convergence is explained by the finite amplitude of the PF pressure jumps in individual mesh cells, which is dictated by thermodynamics and is not mitigated as the mesh is refined. A way out of this predicament would be to split every PF into a sequence of weaker transitions. In this way, one could imitate the physical kinetics of a phase transition, where an MS state decays over a short but finite time during which the fluid manages to accelerate and expand. In the next section, we will discuss a method based on this idea.

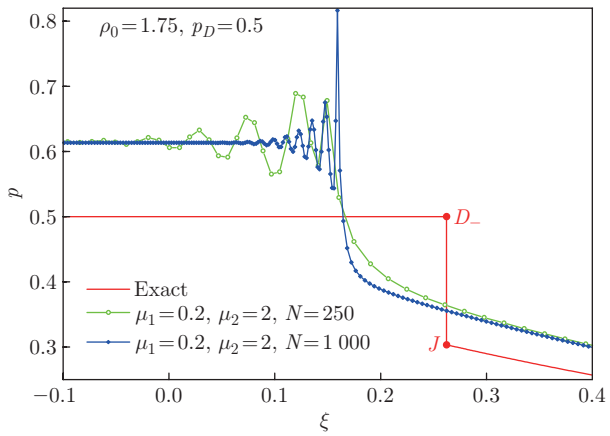

Fig. 3 Pressure profiles in the immediate vicinity of the rarefaction shock for the reference case of Fig. 2. The two numerical profiles (green and blue), calculated for two different grid resolutions, demonstrate a clear absence of convergence to the exact solution (thick red curve) (color online)

3 Method of artificial relaxation of hidden internal energy

3.1 Formulation of the method

As before, we assume that, upon arrival at point D on the spinodal (as indicated in Fig. 1), the EOS in the tracked fluid element is instantaneously switched from the MS branch to the EQ branch. But in contrast to the previous single-leap algorithm, a certain amount e_{pf} of

the internal energy is simultaneously withdrawn from the considered fluid element, and then gradually returned to it over a time interval Δt_{pf}. The value of e_{pf} is adjusted so as to practically nullify the pressure jump that would occur if the phase transition was made at fixed v and e. The withdrawn energy e_{pf} may be thought of as temporarily residing in some hidden degrees of freedom, and the proposed algorithm may be termed as a method of artificial energy relaxation.

For a more precise formulation, we assume for a moment that the caloric part of the parental MS EOS (1), (2) has the form $e = e_{\rm MS}(v, p)$, while its EQ branch is given by the function $e = E_{\rm EQ}(v, p)$. Then, the hidden energy e_{pf} is defined as

$$e_{pf} = e_D - E_{\rm EQ}(v_D, p_{D1}), \tag{4}$$

where v_D, p_D, and $e_D = e_{\rm MS}(v_D, p_D)$ are the thermodynamic parameters of the pre-flip state D, while

$$p_{D1} = \min(p_G, \max(0, p_D) + \delta_p) \tag{5}$$

is the desired pressure immediately after switching to the EQ EOS. In Eq. (5), p_G is the upper limit to the post-flip pressure, which is achieved at point G in Fig. 1 for $e_{pf} = 0$ and must be calculated from the equation

$$E_{\rm EQ}(v_D, p_G) = e_{\rm MS}(v_D, p_D). \tag{6}$$

It is assumed that $p_G \geqslant p_D$, which is always true for the EOS used here. Although one might prefer a perfectly smooth start with $p_{D1} = p_D$ for the relaxation phase, a small initial pressure jump of δ_p ($\in [0.001, 0.1]$) (in units of $P_{\rm cr}$), treated as a free parameter of the algorithm, provides certain practical advantages. Note that for $p_D < 0$, a smooth start with $p_{D1} = p_D$ would be impossible because the EQ EOS does not allow negative pressures.

To redeposit the hidden energy e_{pf}, we introduce an artificial heating term

$$w \equiv w_{pf} = e_{pf}/\Delta t_{pf} \tag{7}$$

into the energy equation (A4). A constant heating rate w_{pf} is applied within the time interval $t_{pf} < t < t_{pf} + \Delta t_{pf}$ to that same Lagrangian cell, where e_{pf} has been removed from the fluid at the starting moment $t = t_{pf}$ of the MS→EQ transition.

When the finite-difference equations are solved, the relaxation time Δt_{pf} must be chosen so as to allow the mesh cell under consideration to expand as it passes through the rarefaction shock. This can be achieved by setting

$$\Delta t_{pf} = \tau_{pf} \min(\Delta t_{xa}, \Delta t_{ss}), \tag{8}$$

where τ_{pf} is a free dimensionless parameter of order unity,

$$\Delta t_{ss} = \Delta x / c_{{\rm s}G} \tag{9}$$

is the sound transit time, calculated with the EQ-EOS sound speed $c_{{\rm s}G}$ in state G, and

$$\Delta t_{xa} = (2\Delta x/a)^{1/2} \tag{10}$$

is the free expansion time, evaluated under the assumption that the pressure difference between the considered cell and the two neighboring cells is equal to its maximum possible increment $p_G - p_D$ in the PF jump. For a mesh cell $\Delta x_{j+1/2} = x_{j+1} - x_j$, the effective acceleration a of its expansion is given by

$$a_{j+1/2} = (p_{G,j+1/2} - p_{D,j+1/2})\Big(\frac{1}{\delta m_j} + \frac{1}{\delta m_{j+1}}\Big), \tag{11}$$

where

$$\delta m_j = \frac{1}{2}(\rho_{j+1/2}\Delta x_{j+1/2} + \rho_{j-1/2}\Delta x_{j-1/2}) \tag{12}$$

is the mass associated with the mesh node j. It is, of course, supposed that, when the numerical scheme from Appendix A is used, all the quantities in Eqs. (4)–(10), except for the two global parameters δ_p and τ_{pf}, bear a spatial index $j + 1/2$.

3.2 Numerical tests

The improvement that can be achieved by introducing artificial energy relaxation is demonstrated by the pressure profiles in Fig. 4, calculated with different values of τ_{pf} in Eq. (8) for the same CRW solution as in Figs. 2 and 3. The profile $\tau_{pf} = 0$ repeats the $N = 250$ curve of Fig. 3 because an infinitely fast energy relaxation is equivalent to the single-leap algorithm of Section 2. Comparison of the $\tau_{pf} = 4$, 8, and 16 profiles with that for $\tau_{pf} = 0$ demonstrates that for $\tau_{pf} \geqslant 4$, the numerical solution becomes significantly closer to the exact one, i.e., the spinodal-shelf pressure approaches its exact value $p_D = 0.5$, the shock front shifts noticeably towards its correct position, and the amplitude of the post-shock oscillations diminishes. At the same time, the error in the numerical profiles becomes rather insensitive to the exact value of τ_{pf} once the latter exceeds 3–4, which attests the robustness of the algorithm. When, however, τ_{pf} is chosen too large (τ_{pf} is larger than 10 in our case), the shock front becomes excessively smeared. In what concerning the role of the second parameter δ_p, the numerical error decreases as δ_p is diminished; in our example with $N = 250$ and $\tau_{pf} = 4$, this dependence saturates and can be ignored for δ_p less than about 0.02.

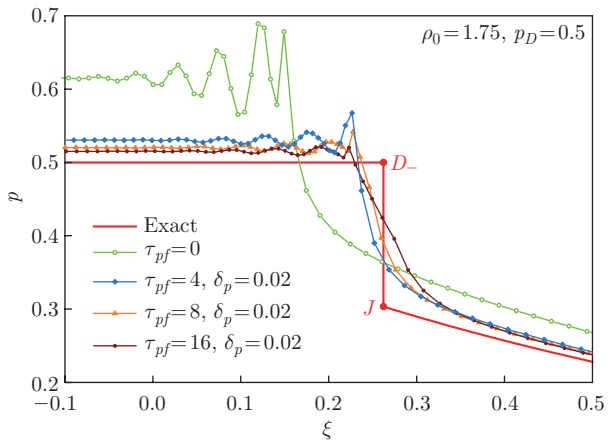

Fig. 4 Pressure profiles in the vicinity of the rarefaction shock for the reference case of Fig. 2, which demonstrate the effect of the artificial energy relaxation for different values of the scale factor τ_{pf} in Eq. (8). In all cases, the coarse mesh with $N = 250$ cells is used. The $\tau_{pf} = 0$ profile repeats the green curve from Fig. 3 (color online)

The artificial energy relaxation opens a way to achieve convergence to the exact solution by a concerted variation of the mesh resolution and the energy relaxation parameters, i.e., as the mesh resolution is increased, one should increase τ_{pf} and decrease δ_p. Because the number of cells, to which the shock front is smeared, is roughly proportional to τ_{pf}, the convergence to an infinitely steep shock front can only be achieved if τ_{pf} is increased more slowly than the total number of cells N, say, as $\tau_{pf} \propto N^{1/2}$. Accordingly, δ_p may be decreased as $\delta_p \propto N^{-1/2}$. The result of applying this procedure to the test case of Figs. 2–4 is shown in Fig. 5, which demonstrates how the deviation from the exact solution diminishes roughly in a direct proportion to $N^{-1/2}$ as the number of cells is increased from $N = 250$ to $N = 1\,000$ and $N = 4\,000$.

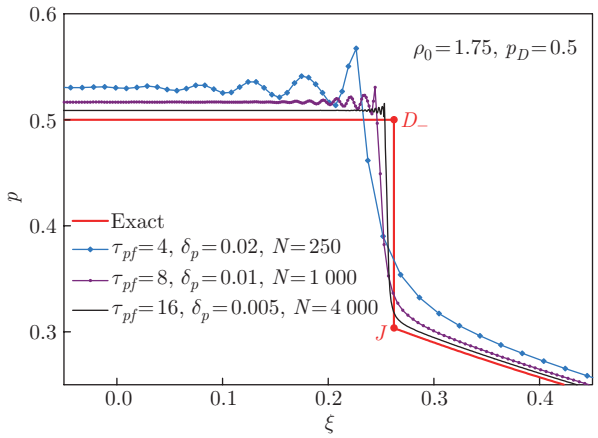

Fig. 5 Convergence to the exact CRW solution, used as a reference case in Figs. 2–4. The convergence is achieved by mesh refinement coordinated with a simultaneous adjustment of the parameters of the artificial energy relaxation. The $N = 250$ pressure profile repeats the blue curve from Fig. 4 (color online)

Note that the exact PF solution discussed here is only marginally stable along its spinodal shelf section D_+D_-, where any perturbation towards a lower pressure would trigger a PF. However, the ensuing compression pulse pushes in the opposite direction, providing stabilization against such a transition in the adjacent flow segments. The latter explains why the spinodal shelves in numerical profiles, where some numerical noise is always present, lie above their exact levels in Figs. 2–5. In this regard, numerical profiles may, in fact, be closer to reality than the idealized exact PF solutions.

Special attention is to be paid to the PF in the limit of vanishing spinodal pressure $p_D \ll 1$. The case of $p_D = 0$ is a bifurcation point, where the PF-CRW solution undergoes a qualitative change, with a rarefaction shock front at $p_D > 0$ being transformed into a sharp boundary between the superheated liquid and vacuum at $p_D < 0$[11]. As $p_D \to +0$, the pressures before and after the shock approach zero, while the density jump $\rho_D/\rho_J \to \infty$ as ρ_D approaches a finite limit and ρ_J vanishes together with the entire flow section behind the shock front.

Figure 6 shows how our numerical algorithm performs in the case of $p_D = 0.05$, where the density jump in the shock is as high as $\rho_D/\rho_J = 60.41$. It is seen that the numerical solution does satisfactorily reproduce the flow characteristics remaining finite in the limit of $p_D \to 0$, like the density on the spinodal shelf and the position of the shock front; but the convergence to the exact solution is noticeably slower than that in the previous reference case of $p_D = 0.5$ with a moderate density jump of $\rho_D/\rho_J = 3.82$, because now the relaxation to a low post-shock density $\rho_J \ll \rho_D$ requires many more hydrodynamic timescales Δt_{pf} than that allowed by an a priori chosen moderate value of τ_{pf}. As a result, the flow parameters in the tenuous post-shock tail are calculated with large relative errors. Note that for $p_D < 0$, where no phase transition takes place, we recover rapid convergence to the exact rarefaction profile, obtained with the stable MS EOS.

Both reference cases, discussed above, have a subcritical entropy of the initial state, for which the expanding fluid passes through the MS region of the superheated liquid and undergoes explosive boiling in the PF rarefaction shock at $v_D < 1$. For supercritical initial entropy, the expanding dry vapor passes through the MS region of supercooled vapor, with a subsequent instantaneous condensation in a rarefaction shock at $v_D > 1$. Because the pre-shock pressure on the vapor branch of the spinodal is always positive, the shock solution

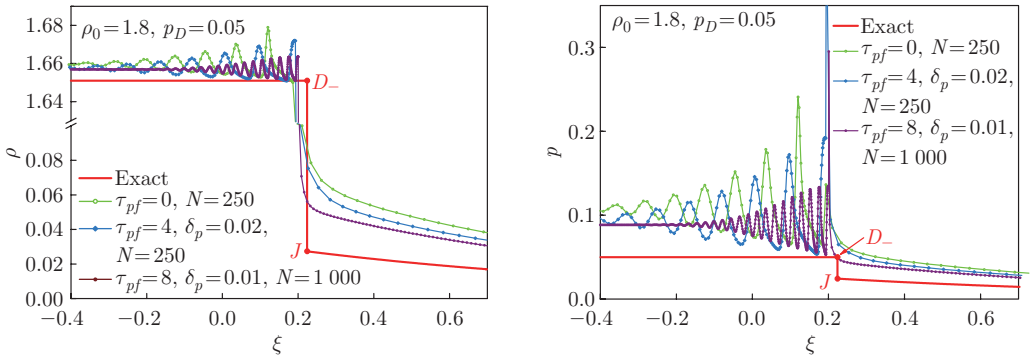

(a) Density (b) Pressure

Fig. 6 Density and pressure profiles for a CRW solution with $\rho_0 = 1.8$ and a close to zero spinodal pressure of $p_D = 0.05$, characterized by a large density jump $\rho_D/\rho_J = 60.41$ in the PF shock. Convergence to the exact solution is noticeably slower than for a moderate density jump in Fig. 5 (color online)

applies to any $v_D > 1$. Figure 7, where the results for a supercritical release isentrope with $\rho_0 = 0.5$ and $v_D = 2.5$ are plotted, demonstrates that the proposed numerical method is no less effective in this case than in the explosive-boiling PF shocks with moderate density jumps.

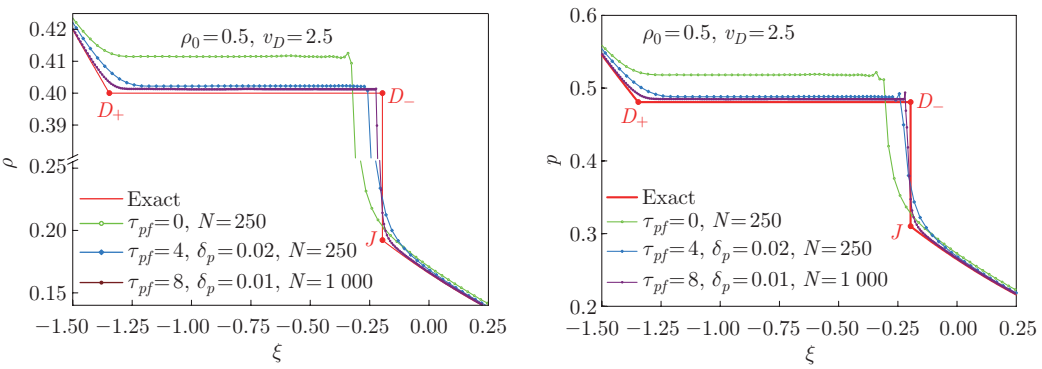

(a) Density (b) Pressure

Fig. 7 Density and pressure profiles in a CRW with a supercritical initial entropy, starting at the initial density $\rho_0 = 0.5$. The expanding dry vapor undergoes a jump-like condensation in a rarefaction shock with the pre-shock spinodal density of $\rho_D = v_D^{-1} = 0.4$. Rapid convergence to the exact solution is confirmed (color online)

4 Conclusions

Based on the assumption of instantaneous decay of MS states on the spinodal, the approximation of PF hydrodynamics opens an attractive and relatively easy way to model fast fluid dynamics with liquid-gas phase transitions[11,15]. However, its numerical implementation requires an adequate technique for capturing a new type of flow discontinuities, of which a particular case is a rarefaction shock that coincides with a "material" interface, separating two thermodynamic phases obeying different EOSs. In the absence of an adequate solution to the corresponding Riemann problem, the modern Godunov-type non-oscillating schemes for multiphase flows cannot be employed to this end, and we are forced to take a step back and revisit the more straight earlier approach of artificial viscosity.

In this paper, we limit our treatment to the Lagrangian framework which saves us the effort to track the MS-EQ phase interface. We begin by ascertaining that the classical von NNR quadratic viscosity cannot satisfy our needs. Then, we show that, once combined with a linear (with respect to the fluid velocity) term and allowed to be operative in both compression and expansion, the scalar artificial viscosity becomes potent enough to effectively suppress strong spurious oscillations, emanated from the rarefaction shock front in both the upstream and downstream directions. However, the artificial viscosity alone fails to ensure convergence to the exact solution in the reference case of a release wave into a vacuum[11]. We demonstrate that the convergence can be restored by adding a new ingredient into the numerical algorithm, i.e., an artificial relaxation term for a fictitious (hidden) component of the internal energy, artificially withdrawn from the fluid elements as they undergo a PF. Similar to the artificial viscosity, the proposed "artificial kinetics" term has two dimensionless parameters, for which reasonably universal values are established.

The conducted numerical tests have demonstrated that the proposed algorithm is robust and stable, and ensures a good accuracy for the PF rarefaction shocks with moderate (within, say, a factor less than 10) density jumps. The numerical errors become larger (but remain limited) as the density jump approaches infinity in the limit of zero pressure in the pre-shock state of an MS superheated liquid. An important advantage of this algorithm is its universality with respect to the employed EOS, especially in view of the fact that the Maxwell construction for the EQ branch of any two-phase EOS cannot be done algebraically. The obvious shortcoming is spurious oscillations behind the shock front which are, in our case, primarily excited by the MS→EQ phase transition. Unfortunately, no comparison with any oscillation-free Godunov-type scheme can be performed at this stage because such schemes have not yet been developed for the explored type of hydrodynamic discontinuity, for which a proper general analysis of the Riemann problem is still lacking.

Although tested in the 1D planar geometry only, the proposed method is easily generalized to higher dimensions within the Lagrangian framework. Generalization to Eulerian (or arbitrary Lagrangian-Eulerian) schemes is more problematic as it would require new techniques for simultaneous treatment of two thermodynamic phases out of EQ with one another in the same mesh cell.

References

[1] SOKOLOWSKI-TINTEN, K., BIALKOWSKI, J., CAVALLERI, A., VON DER LINDE, D., OPARIN, A., MEYER-TER-VEHN, J., and ANISIMOV, S. I. Transient states of matter during short pulse laser ablation. *Physical Review Letters*, **81**, 224–227 (1988)

[2] INOGAMOV, N. A., ANISIMOV, S. I., and RETHFELD, B. Rarefaction wave and gravitational equilibrium in a two-phase liquid-vapor medium. *Journal of Experimental and Theoretical Physics*, **88**, 1143–1150 (1999)

[3] AGRANAT, M. B., ANISIMOV, S. I., ASHITKOV, S. I., ZHAKHOVSKII, V. V., INOGAMOV, N. A., KOMAROV, P. S., OVCHINNIKOV, A. V., FORTOV, V. E., KHOKHLOV, V. A., and SHEPELEV, V. V. Strength properties of an aluminum melt at extremely high tension rates under the action of femtosecond laser pulses. *JETP Letters*, **91**, 471–477 (2010)

[4] BASKO, M. M., KRIVOKORYTOV, M. S., VINOKHODOV, A. Y., SIDELNIKOV, Y. V., KRIVTSUN, V. M., MEDVEDEV, V. V., KIM, D. A., KOMPANETS, V. O., LASH, A. A., and KOSHELEV, K. N. Fragmentation dynamics of liquid-metal droplets under ultra-short laser pulses. *Laser Physics Letters*, **14**, 036001 (2017)

[5] BRENNEN, C. E. *Cavitation and Bubble Dynamics*, Oxford University Press, New York (1995)

[6] UTKIN, A. V., SOSIKOV, V. A., BOGACH, A. A., and FORTOV, V. E. Tension of liquids by shock waves. *AIP Conference Proceedings*, **706**, 765–770 (2004)

[7] DE RESSÉGUIER, T., SIGNOR, L., DRAGON, A., BOUSTIE, M., ROY, G., and LLORCA, F. Experimental investigation of liquid spall in laser shock-loaded tin. *Journal of Applied Physics*, **101**, 013506 (2007)

[8] STAN, C. A., WILLMOTT, P. R., STONE, H. A., KOGLIN, J. E., LIANG, M., AQUILA, A. L., ROBINSON, J. S., GUMERLOCK, K. L., BLAJ, G., SIERRA, R. G., BOUTET, S., GUILLET, S. A. H., CURTIS, R. H., VETTER, S. L., LOOS, H., TURNER, J. L., and DECKER, F. J. Negative pressures and spallation in water drops subjected to nanosecond shock waves. *The Journal of Physical Chemistry Letters*, **7**, 2055–2062 (2016)

[9] COLOMBIER, J. P., COMBIS, P., BONNEAU, F., LE HARZIC, R., and AUDOUARD, E. Hydrodynamic simulations of metal ablation by femtosecond laser irradiation. *Physical Review B*, **71**, 165406 (2005)

[10] ZHAO, N., MENTRELLI, A., RUGGERI, T., and SUGIYAMA, M. Admissible shock waves and shock-induced phase transitions in a van der Waals fluid. *Physics of Fluids*, **23**, 086101 (2011)

[11] BASKO, M. M. Centered rarefaction wave with a liquid-gas phase transition in the approximation of "phase-flip" hydrodynamics. *Physics of Fluids*, **30**, 123306 (2018)

[12] BLANDER, M. and KATZ, J. L. Bubble nucleation in liquids. *AIChE Journal*, **21**, 833–848 (1975)

[13] MARTYNYUK, M. M. Phase explosion of a metastable fluid. *Combustion, Explosion and Shock Waves*, **13**, 178–191 (1977)

[14] SKRIPOV, V. P. and SKRIPOV, A. V. Spinodal decomposition (phase transitions via unstable states). *Soviet Physics Uspekhi*, **22**, 389–410 (1979)

[15] FAIK, S., BASKO, M. M., TAUSCHWITZ, A., IOSILEVSKIY, I., and MARUHN, J. A. Dynamics of volumetrically heated matter passing through the liquid-vapor metastable states. *High Energy Density Physics*, **8**, 349–359 (2012)

[16] GRADY, D. E. Spall and fragmentation in high-temperature metals. *High Pressure Shock Compression of Solids* II: *Dynamic Fracture and Fragmentation* (eds. DAVISON, L., GRADY, D. E., and SHAHINPOOR, M.), Springer, New York, 219–236 (1996)

[17] SAUREL, R., PETITPAS, F., and ABGRALL, R. Modelling phase transition in metastable liquids: application to cavitating and flashing flows. *Journal of Fluid Mechanics*, **607**, 313–350 (2008)

[18] ZEIN, A., HANTKE, M., and WARNECKE, G. Modeling phase transition for compressible two-phase flows applied to metastable liquids. *Journal of Computational Physics*, **229**, 2964–2998 (2010)

[19] CAI, Y., WU, H. A., and LUO, S. N. Spall strength of liquid copper and accuracy of the acoustic method. *Journal of Applied Physics*, **121**, 105901 (2017)

[20] MAYER, A. E. and MAYER, P. N. Strain rate dependence of spall strength for solid and molten lead and tin. *International Journal of Fracture*, **222**, 171–195 (2020)

[21] FARHAT, C., GERBEAU, J. F., and RALLU, A. FIVER: a finite volume method based on exact two-phase Riemann problems and sparse grids for multi-material flows with large density jumps. *Journal of Computational Physics*, **231**, 6360–6379 (2012)

[22] SHAHBAZI, K. Robust second-order scheme for multi-phase flow computations. *Journal of Computational Physics*, **339**, 163–178 (2017)

[23] ZHANG, C. and MENSHOV, I. Eulerian model for simulating multi-fluid flows with an arbitrary number of immiscible compressible components. *Journal of Scientific Computing*, **83**, 31 (2020)

[24] MARTYNYUK, M. M. Generalized van der Waals equation of state for liquids and gases. *Zhurnal Fizicheskoi Khimii* (*Russian Journal of Physical Chemistry A*), **65**, 1716–1717 (1991)

[25] MARTYNYUK, M. M. Transition of liquid metals into vapor in the process of pulse heating by current. *International Journal of Thermophysics*, **14**, 457–470 (1993)

[26] BASKO, M. M. Generalized van der Waals equation of state for in-line use in hydrodynamic codes. *Keldysh Institute Preprints* (2018) https://doi.org/10.20948/prepr-2018-112-e

[27] RICHTMYER, R. D. and MORTON, K. W. *Difference Methods for Initial-Value Problems*, 2nd ed., Interscience Publishers, New York (1967)

[28] LANDAU, L. D. and LIFSHITZ, E. M. *Fluid Mechanics*, 2nd ed., Pergamon Press, Oxford (1987)

[29] ZEL'DOVICH, Y. B. and RAIZER, Y. P. *Physics of Shock Waves and High-Temperature Hydrodynamic Phenomena*, Dover Publications, New York (2012)

[30] MATTSSON, A. E. and RIDER, W. J. Artificial viscosity: back to the basics. *International Journal for Numerical Methods in Fluids*, **77**, 400–417 (2015)

[31] LANDSHOFF, R. *A Numerical Method for Treating Fluid Flow in the Presence of Shocks*, Report LA-1930, Los Alamos National Laboratory, Los Alamos (1955)

[32] VON NEUMANN, J. and RICHTMYER, R. D. A method for the numerical calculation of hydrodynamic shocks. *Journal of Applied Physics*, **21**, 232–237 (1950)

[33] BASKO, M. M., SASOROV, P. V., MURAKAMI, M., NOVIKOV, V. G., and GRUSHIN, A. S. One-dimensional study of the radiation-dominated implosion of a cylindrical tungsten plasma column. *Plasma Physics and Controlled Fusion*, **54**(5), 055003 (2012)

Appendix A Finite-difference scheme used in numerical tests

With respect to the Lagrangian variable

$$m = \int_0^x \rho \, \mathrm{d}x, \tag{A1}$$

the equations of 1D plane-parallel hydrodynamics can be written as[29]

$$\frac{\partial x}{\partial t} = u, \tag{A2}$$

$$\frac{\partial u}{\partial t} + \frac{\partial}{\partial m}(p+q) = 0, \tag{A3}$$

$$e_T \frac{\partial T}{\partial t} + (p + q + e_v)\frac{\partial u}{\partial m} = w, \tag{A4}$$

where the principal dependent variables are the position $x = x(t, m)$, the velocity $u = u(t, m)$, and the temperature $T = T(t, m)$ of a fluid element m. The EOS is assumed to be given in the form as follows:

$$p = p(v, T), \quad e = e(v, T), \quad e_T \equiv \frac{\partial e}{\partial T}, \quad e_v \equiv \frac{\partial e}{\partial v}.$$

q is the artificial viscosity (3), w is the rate of eventual external heating, and the specific volume v is given by

$$v = \frac{\partial x}{\partial m}. \tag{A5}$$

Equations (A2)–(A4) and the numerical scheme below, where the temperature T is chosen as the principal dependent energy variable, constitute an abridged version of the 1D model implemented in the three-temperature DEIRA code[33], which, in particular, includes the heat conduction terms.

Once a discrete grid $\{m_j\}$ $(j = 1, 2, \cdots, N+1)$ of N Lagrangian cells is set, the kinematic variables x and u are assigned to cell nodes with integer indices $j, j \pm 1$, while the thermodynamic variables v, p, q, T, e_T, e_v, and c_s are attributed to cell centers with half-integer indices $j \pm 1/2$. Then, the numerical scheme used in this work is given by

$$\frac{\bar{x}_j - x_j}{\Delta t} = \frac{1}{2}\left(u_j + \bar{u}_j\right), \tag{A6}$$

$$\frac{\bar{u}_j - u_j}{\Delta t} + 2\frac{p_{j+1/2} + \tilde{q}_{j+1/2} - p_{j-1/2} - \tilde{q}_{j-1/2}}{m_{j+1} - m_{j-1}} = 0, \tag{A7}$$

$$e_{T,j+1/2}\frac{\overline{T}_{j+1/2} - T_{j+1/2}}{\Delta t} + \left(p_{j+1/2} + \tilde{q}_{j+1/2} + e_{v,j+1/2}\right)\frac{\widetilde{\Delta u}_{j+1/2}}{m_{j+1} - m_j} = w_{j+1/2}, \tag{A8}$$

where

$$\tilde{q}_{j+1/2} = -\frac{\mu_1 c_{\mathrm{s},j+1/2} + \mu_2 |u_{j+1} - u_j|}{v_{j+1/2}} \, \widetilde{\Delta u}_{j+1/2}, \tag{A9}$$

$$\widetilde{\Delta u}_{j+1/2} = \frac{1}{2} \left(u_{j+1} + \bar{u}_{j+1} - u_j - \bar{u}_j \right). \tag{A10}$$

With respect to time discretization, the old values x and u are centered at t_n, while the new ones with a bar, i.e., $\bar{x}$ and $\bar{u}$, are centered at $t_{n+1} = t_n + \Delta t$. The old values v, p, T, e_T, e_v, and c_s and the intermediate values $\tilde{q}$ and $\widetilde{\Delta u}$ are assumed to be centered at $t_{n+1/2}$. Accordingly, the new temperatures $\overline{T}$ in Eq. (A8) and the new specific volumes

$$\bar{v}_{j+1/2} = \frac{\bar{x}_{j+1} - \bar{x}_j + \frac{1}{2} \left(\bar{u}_{j+1} - \bar{u}_j \right) \Delta t}{m_{j+1} - m_j} \tag{A11}$$

are centered at $t_{n+3/2}$.

Apart from the quadratic viscosity term $\mu_2 |u_{j+1} - u_j|$ in Eq. (A9), Eqs. (A6) and (A7) are correctly centered to provide the second-order accuracy in time and space, while the energy equation (A8) remains to be of the first-order in time. At each time step, the system of linear equations in Eq. (A7) for the unknown $\bar{u}_j$ can be solved by applying the tridiagonal matrix algorithm, after which all the other new quantities are easily found. The above numerical scheme is stable for the values of the CFL number

$$L \equiv \max_j \left\{ \frac{c_{\mathrm{s},j+1/2} \, \Delta t}{x_{j+1} - x_j} \right\} < 0.5. \tag{A12}$$